European Commission

JRC TECHNICAL REPORTS

Image analysis in nuclear forensics

The use of image texture analysis for the identification of uranium ore concentrate samples: new perspective in nuclear forensics

Lorenzo Fongaro, Vincenzo Rondinella, Klaus Mayer

2016

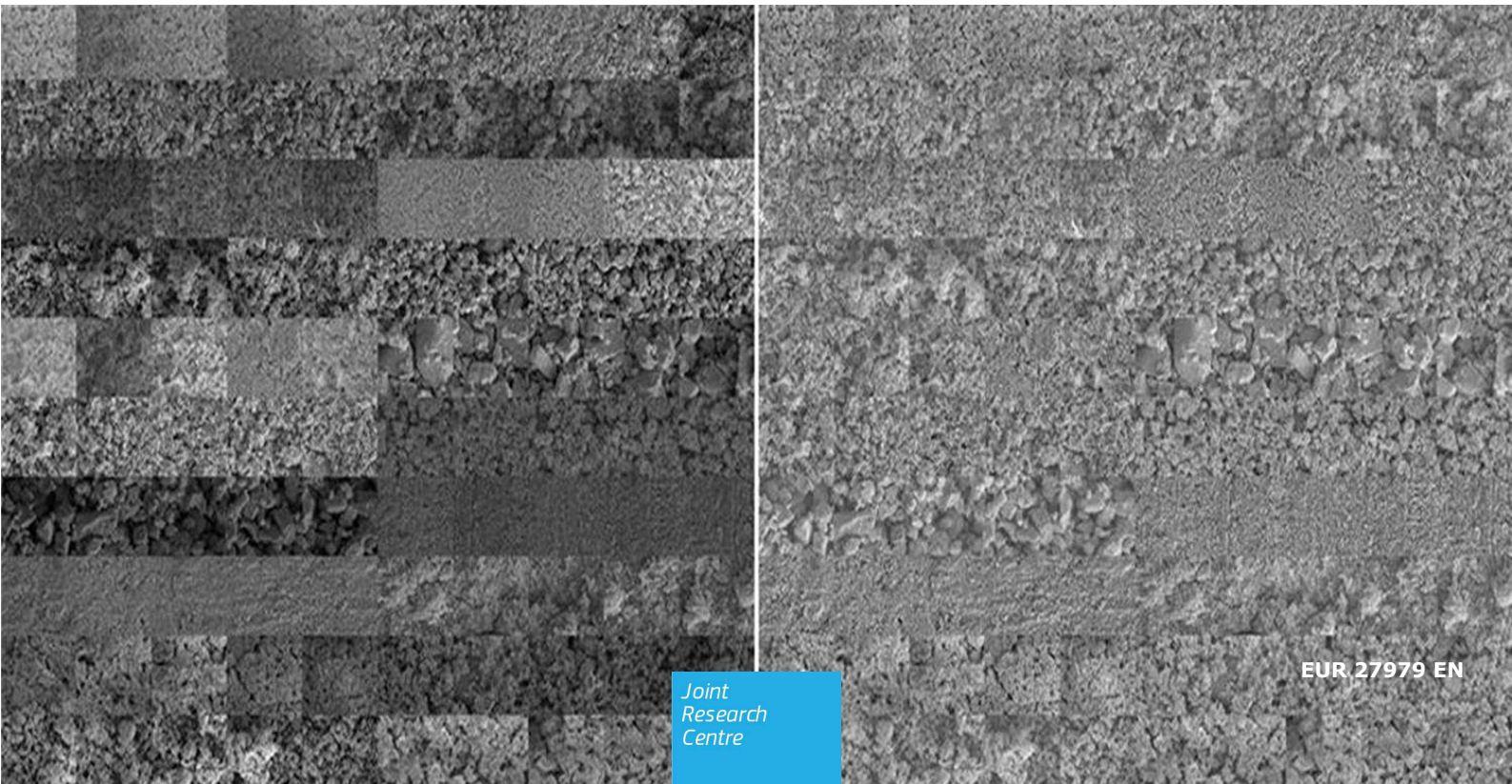

Joint Research Centre

EUR 27979 EN

Image analysis in nuclear forensics

Contact information
Name: Lorenzo Fongaro
Address: P.O. Box 2340, 76125 Karlsruhe/Germany
Email: lorenzo.fongaro@ec.europa.eu
Tel. +49 7247951593

JRC Science Hub
https://ec.europa.eu/jrc

JRC101497

EUR 27979 EN

ISBN 978-92-79-59538-7 (PDF)
ISBN 978-92-79-59539-4 (print)

ISSN 1831-9424 (online)
ISSN 1018-5593 (print)

doi:10.2789/851269 (online)
doi:10.2789/226321 (print)

Printed in Karlsruhe *(Germany)*

How to cite: Fongaro et al. (2016), Image analysis in nuclear forensics, EUR 27979 EN; doi 10.2789/851269

Contents

Acknowledgements

The authors wish to acknowledge the precious contribution of Dr Ho Mer Lin Doris as this technical report is a part of the results of her PhD.

Abstract

In this technical report, a new approach for characterising powder of uranium ore concentrates (UOCs) is presented. It is based on image texture analysis and multivariate data modelling. Twenty-six different UOC samples were evaluated, applying the angle measure technique (AMT) algorithm to extract textural features on samples images acquired at 250× and 1 000× magnification by scanning electron microscope (SEM). At both magnifications, this method proved effective to classify the different types of UOC powder based on the surface characteristics that depend on particle size, homogeneity, and graininess and are related to the composition and processes used in the production facilities. Using the outcome data from the application of the AMT algorithm, the total explained variance was higher than 90 % with principal component analysis (PCA). This preliminary study shows that this method is able to distinguish samples with similar composition, but obtained from different facilities. The mean angle spectral data obtained by the image texture analysis using the AMT algorithm can be considered as a specific fingerprint or signature of UOCs and could be used for nuclear forensic investigation.

1. Introduction

In the event of a discovery of illicit trafficking of nuclear material, questions such as 'what is the material?', 'How it was produced?', 'Where did it come from?', have to be answered as soon as possible. Typically, an investigation involves several measurable parameters, also termed signatures or fingerprints; these can be understood as physical, chemical, isotopic characteristics of the nuclear materials that could collectively help to identify its origin [1-4].

Uranium ore concentrates (UOCs), or 'yellow cakes', are the precursors of nuclear fuel. These materials are often traded in large quantities and, therefore, diversions or thefts can happen. In fact, nuclear forensic investigations have been reported on this type of material [5-7]. Various measurable quantities associated with yellow cake compositions have been reported. These include analysis of major isotopes of uranium, minor isotopes, other minor constituents, non-volatile organics and anionic impurities [8-21]. Spectroscopic techniques such as infrared [21], near infrared reflectance [22, 23], laser-induced breakdown [24] and Raman [25-26] of 'yellow cakes' have also been applied.

A less explored signature is the correlation between the morphological characteristics of different UOCs, obtained using image analysis (IA) technique, and the processing or production history. IA represents a valid tool for the scientists that has been used in a wide range of fields [27-30] and that is currently gaining popularity in the nuclear field [31-33]. Several qualitative and quantitative methods have been applied to images of nuclear materials for different purposes [34-36]. This technique allows the rapid definition of morphological and intensity characteristics of an object or of a complex structure in terms of size, shape, colour or surface properties (surface texture). Keegan et al. [7], for instance, described qualitatively the morphology of samples from two different UOCs; the physical examination was conducted using both optical and electron microscopy and the samples revealed a difference in the microstructure of smaller grains; in particular, in one case the smaller grains exhibited rougher, 'more textured' morphology, while in the other the grains were smoother, showing 'less textured' morphology. This difference in microstructure, as explained by Keegan, might be evidence of a different processing history for the two materials. Recently, Ho Mer Lin et al. have demonstrated that IA can be used as an analytical technique to identify and classify several different UOC samples on the basis of their morphology characteristics [37].

Among the different methods, image texture analysis is gaining interest with scientists for powder characterisation [38]; this is because these methods provide information not only on the individual particles, but also on the bulk powder environment (i.e. how the particles are arranged together). Traditional IA for powder characterisation is instead focused on single particle analysis; moreover, this approach requires time-consuming steps for sample preparation, e.g. for dispersion of the powder, before microscopic imaging [7, 39].

The aim of this report is to show the ability of the image texture analysis to identify different powders of UOCs from their surface appearance (surface topography, surface texture). The angle measure technique (AMT) [40, 41] algorithm was applied, as part of the image texture analysis methods, to 26 UOCs from 26 separate facilities located in various countries. The surface appearance of the powder samples of the UOCs is influenced by the composition and the process technology [7], which give rise to different chemical–physical properties such as grain size, shape, homogeneity, etc. and to the capacity to create agglomerates of different dimension. All these features were evaluated by the assessment of the image texture.

2. Methodology

2.1 Powder samples

A total of 26 UOC samples were selected on the basis of their composition and the technology used for the production (Table 1). The samples were prepared in the following way: a few hundred milligrams of powder were placed in a clean petri dish; a layer of adhesive carbon (sticky on both sides) was applied onto a 12.5 mm SEM sample disk holder; the holder coated by the double sticky tape was put in contact with the sample powder. The holder was gently pressed onto the sample until sufficient powder adhered to the tape. The samples were subsequently coated with 10 nm gold to ensure conductivity in view of the scanning electron microscopy examination.

2.2 Image analysis (IA)

2.2.1 Image acquisition

From each of the 26 samples holders, five images with a dimension of 2 560 × 2 320 pixels were acquired at two different magnifications, 250× and 1 000× (10 images/sample holder), using a scanning electron microscope (SEM) VEGA-TESCAN TS5130LSH from Oxford Instruments. From the two sets of 130 photos at 250× and 1 000×, two stacks (PRE-STACK250×, PRE-STACK1000×) with dimensions of 2 450 × 1 850 pixels were generated and cropped. Each PRE-STACK is constituted by the sequence of the 130 images corresponding to one magnification. On each image belonging to one PRE-STACK, four regions of interest (ROI) of 1 000 × 800 pixels were selected and cropped at four different positions in such a way that almost the entire surface of the original image was covered. In this way, four sub-samples labelled stack1m, stack2m, stack3m, and stack4m (where m=250× or 1 000×) were obtained for each of the two PRE-STACKs. The dimensions of each ROI correspond to 432.9 × 346.32 µm (149 921.92 µm2) and 108.23 × 86.58 µm (9 370.55 µm2) for the images acquired at 250× and 1 000×, respectively. Figures 1 and 2 show the positions of the four ROIs used to create each stackm and all the images composing stack1m. Each stackm comprising 130 images was then pre-processed and analysed separately. As the images exhibited big differences in the mean intensity level, it has been necessary to pre-process the stacks in terms of mean centring and grey level ranges (0-255) in order to eliminate this effect. For this purpose a specific script for ImageJ v. 1.48 (ImageJ, U.S. National Institutes of Health, Bethesda, Maryland, USA, http://imagej.nih.gov/ij) [42] was used to mean centre the images. An example of the normalisation is showed in Figure 3: it is evident that the samples appearance has become more uniform. All the stacks were also reduced in dimensions before the analysis, as proposed by Kucheryavski et al. (2008) [43], and resized to 500 × 400 pixels in length and width respectively, in order to reduce the length of analysis.

Table 1. Information on the 26 UOC samples investigated in this study.

Facility and abbreviation	Country	Composition ([1])	Known processes
South Alligator (ALL)	Australia	Uranyl hydroxide	U ppt with MgO
Atlas (Atl)*	USA	U_3O_8	U ppt with H_2O_2
Chevron Hill (ChH)	USA	Mixed (ADU+oxide)	U ppt with NH_3
Congo (Con)	Belgium	Uranyl hydroxide	Not known/available
South Dakota (Dak)	USA	Mixed (oxide + hydroxide)	U ppt with MgO
ESI (ESI)	Canada	ADU	U ppt with NH_3
ESI (ES2)	USA	ADU	Not known/available
El Dorado (ElD)	Canada	ADU	U ppt with NaOH
Federal American Partners (FAP)*	USA	U_3O_8	U ppt with NH_3
Heng Yang*	China	UO_2 (+ U_3O_8)	Not known/available
Key Lake (KeL)*	Canada	U_3O_8	U ppt+NH_3, calcined at 750 °C
Mary Kathleen (MaK)*	Australia	U_3O_8	U ppt with NH_3
Mulberry (Mul)	USA	ADU	Not known/available
Nufcor (Nuf)*	S. Africa	U_3O_8	Not known/available
Olympic Dam (OlD)*	Australia	U_3O_8	U ppt+NH_3, ADU dried/calcined at 750 °C
Palabora (Pal)*	S. Africa	U_3O_8	U ppt with NH_3
Petromics (Pet)*	USA	Mixed oxide	Not known/available
Queensland (Que)*	Australia	U_3O_8	U ppt with NH_3
Rabbit Lake (RaL)	Canada	Uranyl peroxide	U ppt with magnesia and H_2O_2
Ranstad (Ran)	Sweden	Sodium diuranate	U ppt with NaOH
Rössing (Rss)*	Namibia	U_3O_8	U ppt with NH_3
South Uranium Plant (SUP)*	S. Africa	U_3O_8	U ppt + NH_3, calcined at 490 °C for 6 h
Somair (Som)	Niger	Sodium diuranate	U ppt with NaOH
Spisak Black (SpB)*	Yugoslavia	Uranyl hydroxide	Not known/available
Techsnab (Tec)*	Russia	Mixed (U_3O_8 + ADU)	Not known/available
United Nuclear (UnN)	USA	ADU	Not known/available

([1]) The compositions are assumed from their corresponding infrared and/or Raman spectra.

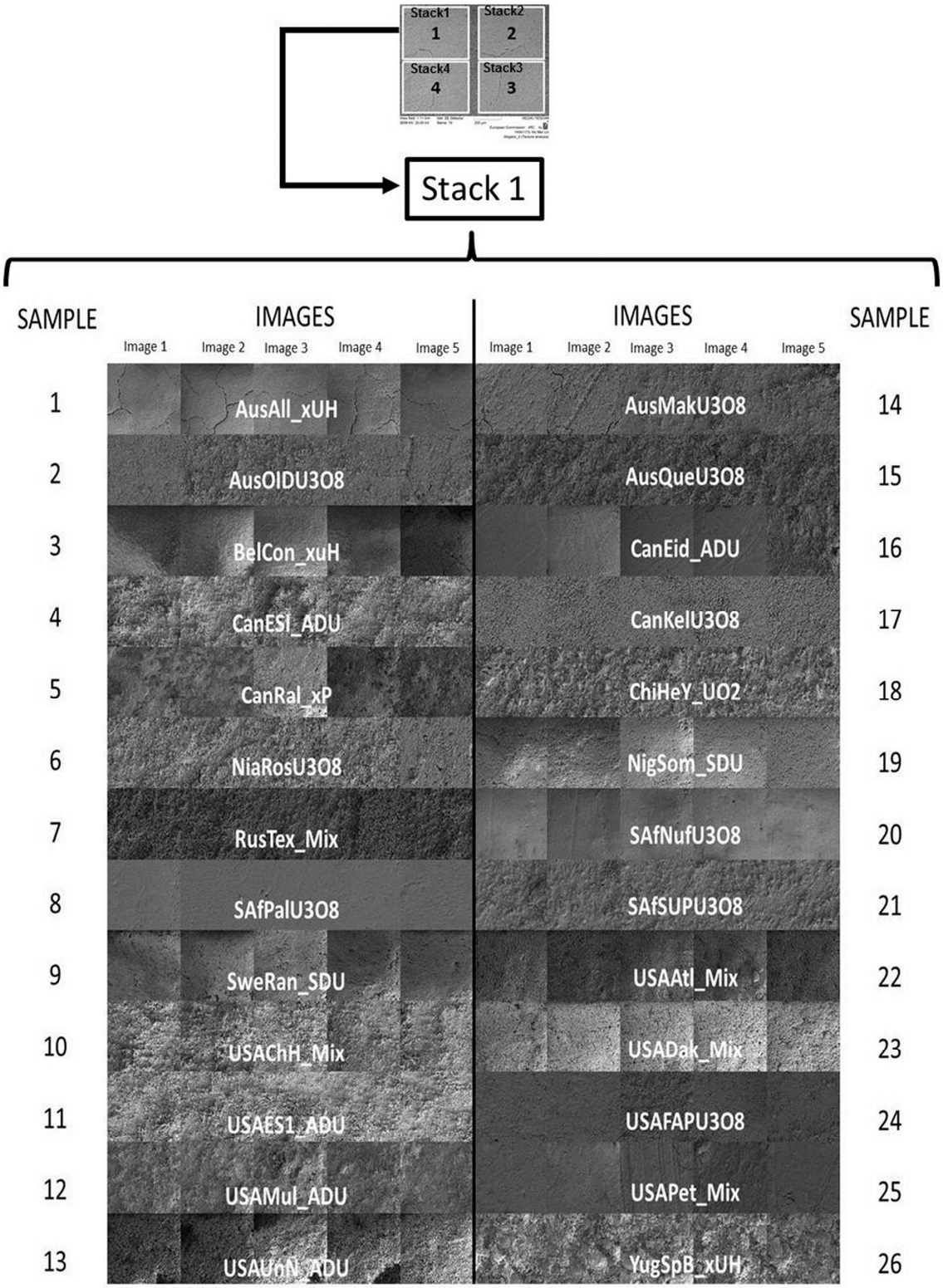

Figure 1. Configuration of images data set at 250×: top, original PRE-STACK of 2 450 × 1 850 pixels with the four different positions from which the region of interest (ROI) subsamples images of 1 000 × 800 pixels were taken; bottom, all the images belonging to stack1$_{250\times}$.

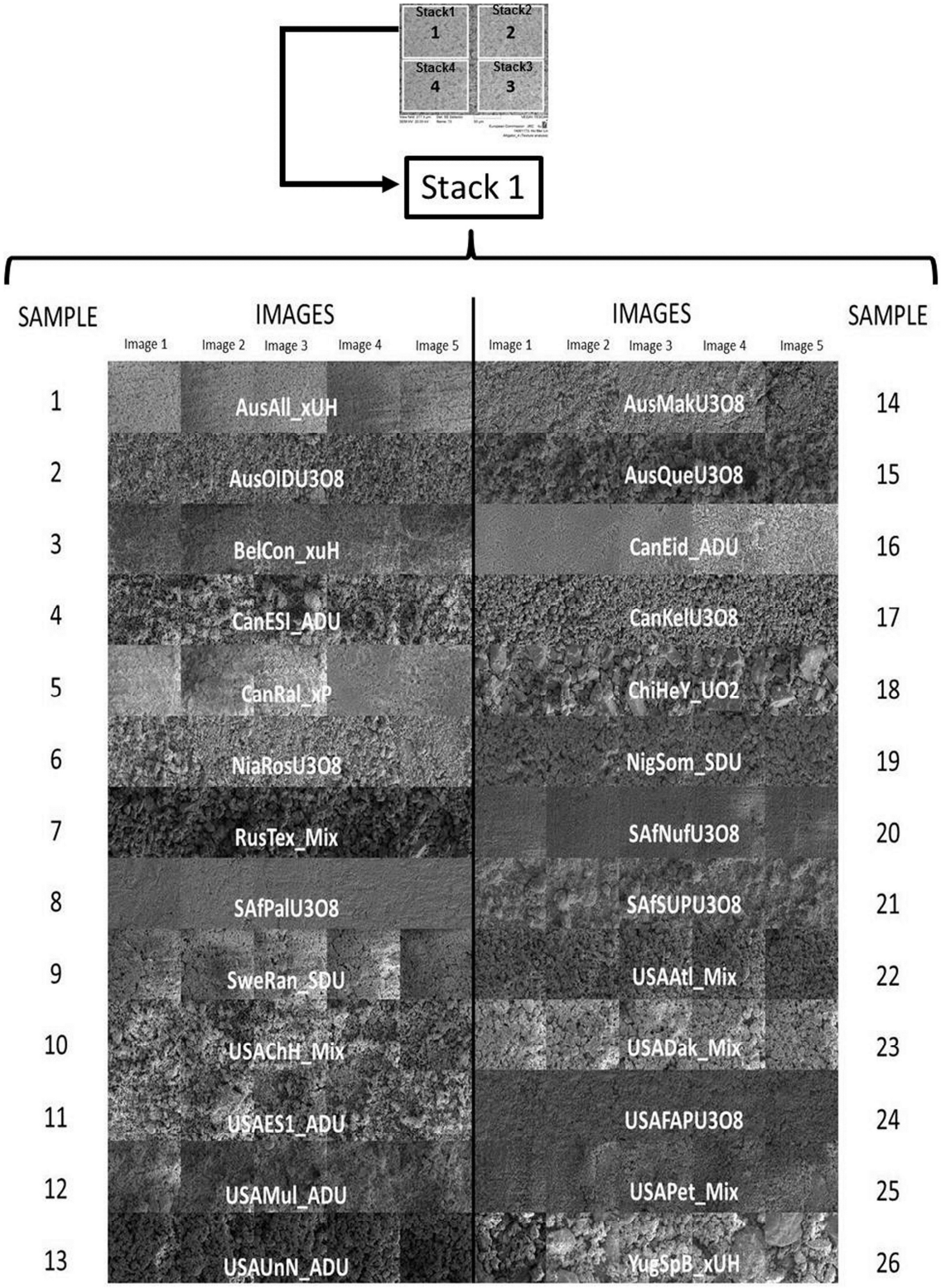

Figure 2. Configuration of images data set at 1 000×: top, original PRE-STACK of 2 450 × 1 850 pixels with the four different positions from which the region of interest (ROI) subsamples images of 1 000 × 800 pixels were taken; bottom, all the images belonging to $stack1_{1000\times}$.

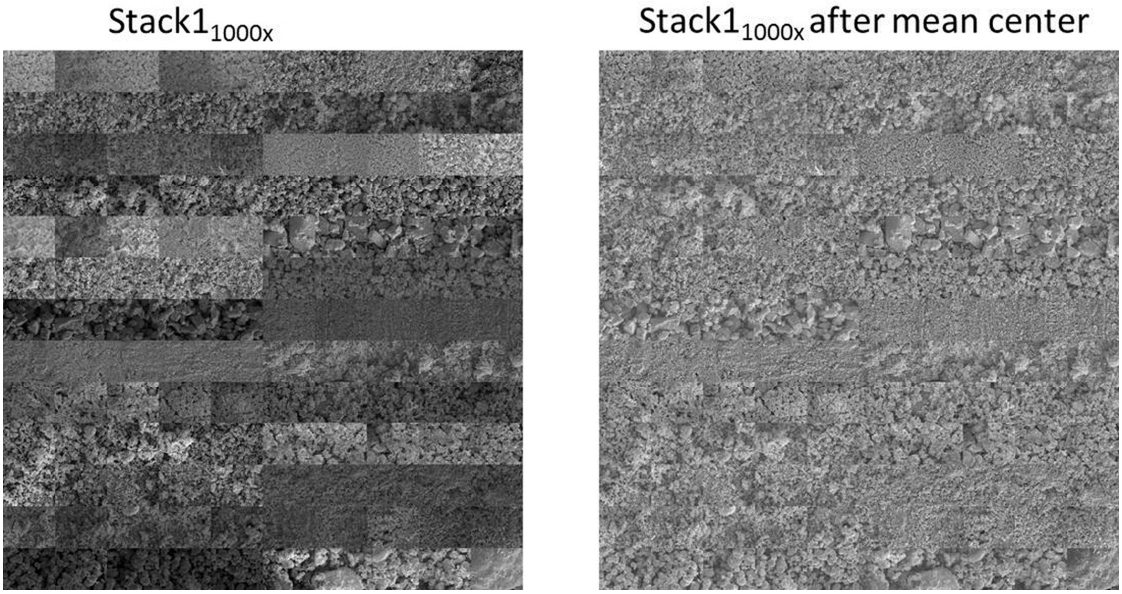

Figure 3. Images of stack1$_{1000x}$ before and after mean centre intensity correction.

2.2.2 Image texture analysis and angle measure technique (AMT)

There are different definitions of image texture, but in general this property of an image is highly dependent on the physical surface characteristic of the object analysed (surface topography, morphology, surface texture) and it could be defined as the spatial distribution, frequency and grey level value of each pixel composing the image [38,39, 41, 43-46]. The term 'surface texture' is generally used to describe the surface appearance of the materials using features that can also be perceived and evaluated through visual inspection of the objects or their images. Surfaces can appear smooth, rough, grainy, etc. and the differences detected can be related to differences in colour or differences in surface topography [45].

In recent years the use of AMT, for surface texture characterisation of different materials, has increased, thanks in particular to its sensitivity in detecting small differences in the surface appearance of different samples [38, 39, 45, 47-49]. The AMT algorithm was used in conjunction with chemo metrics, for the characterisation of signal and texture complexities of images, at different scales [40-41].

The AMT algorithm is based on different steps as illustrated in Figure 4. A detailed description of the AMT algorithm and its implementation and optimisation has been reported elsewhere [40, 41, 43, 50].

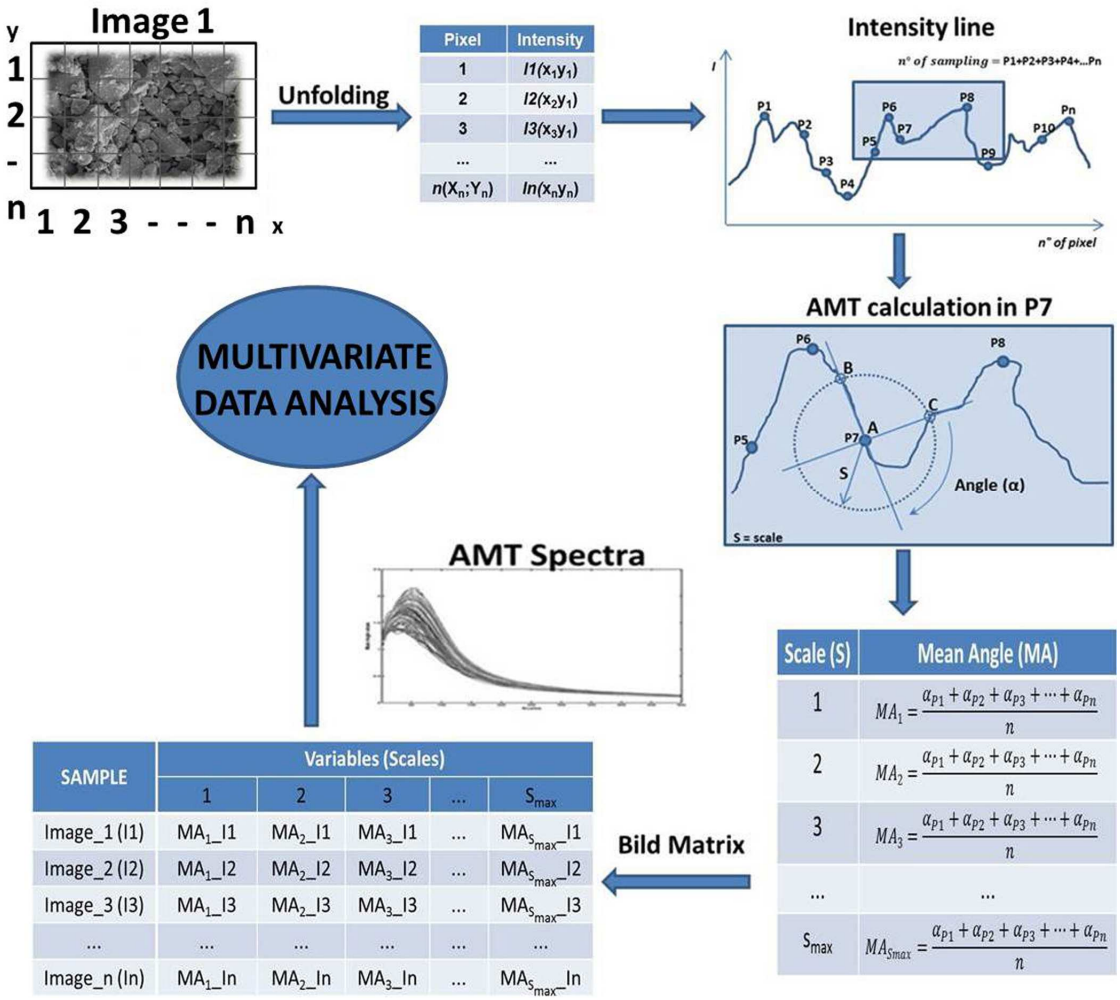

Figure 4. Schematic illustration of the AMT algorithm. The individual angle is measured as the supplement to angle CAB.

In this application, a maximum *s* of 500 pixels and a sampling of 4 000 points, corresponding to 2 % of the total pixels in the images, were used for the AMT algorithm. Calculation of the AMT spectra was done using the jAMTExplorer, an ImageJ plugin implementation of the AMT algorithm [50-52].

2.3 Multivariate data analysis

A PLS Toolbox 7.5.2 (Eigenvectors Research, Inc., USA) for MatLab v. 7.8.0 (The MathWorks Inc., Natick, MA, US) software was used for principal component analysis (PCA). PCA was used here for qualitative analysis of the outcome data from the application of the AMT algorithm on UOCs SEM images; as internal cross validation, the continuous block method was applied using a data split of five due to the number of replicates for each sample in the matrix. For the pre-processing of MA data prior to PCA analysis, mean centre was used [26,45,53-56].

3. Results and discussion

Qualitative results were produced by the evaluation of the surface texture using the AMT method. PCA was carried out on the matrices of the mean angle spectral data obtained from the four different $stacks_m$ at each magnification. The results obtained for 1 000× and for 250× were similar; the total variance explained for the eight PCA considered, has been at least 90 % with the two first PCs. Therefore, the results are confined to $stack1_{1000x}$ and $stack1_{250x}$ in which the optimal results (highest values of explained variance of PC1-PC2) were obtained.

3.1 Results on images at 1 000× magnification

Figure 5 shows the PC1-PC2 scores plots and the relative loading plots for stack1. After the analysis, all 26 samples are shown in the score plot; in particular, seven different symbols have been used to represent them (and their replicates) as a function of their composition, while 26 labels have been used to indicate the relative facilities used for the production. The final PCA results were obtained after reduction of the spectral range to a scale value of 260 and elimination of the outliers (high Q and T^2 values): the first two principal components (PCs) were enough to explain the samples distribution in function of their surface characteristics only. The total explained variance was 96.9 % ($PC1_{S1}$=93.1 %; $PC2_{S1}$=3.8 %).

Looking at the scores plot in Figure 5A, it is possible to identify sample clusters; in particular, those with a surface characterised with a less textured morphology are more concentrated on the right side of the score plot, while the samples characterised by higher textured morphology tend to be on the left part. The samples Tec, Que, SUP, Nuf, ElD, UnN, HeY, SpB, Pal, KeL, can be identified while the others are more overlapped. This behaviour could be explained by the sample preparation procedure, as described in Section 2.1, where small differences in the pressure applied to catch the powder with the sample holder may affect the surface texture. In order to see an average behaviour, PCA was also applied on the mean matrix calculated from the mean angle spectral data matrix of $stack1_{1000x}$. The resulting matrix was formed with only 26 samples. In this case, as internal cross validation, the leave-one-out method was used. The score plot is reported in Figure 5B and all the 26 samples can be easily identified. The samples distribution in the score plot depends always on their surface texture and exhibits good reproducibility, as all replicates of one sample have shown the same behaviour. The image texture of the samples images decreases from the right to the left along the PC1 axis. The closer together the samples are, the more similar they are in terms of surface appearances; this implies that it would be more difficult to identify their origin and composition using only their image. On the contrary, when the samples are sufficiently spread out in the score plot, this means that they have different surface texture morphology (and then different image texture) and this feature can be used for their qualitative identification in term of technology/origin and/or composition. The loadings plot confirms that low scales have stronger influence on the relative position of samples in the scores plot along PC1/PC2, up to a scale of ~ 75; thereafter, a gradual decrease in this effect is observed.

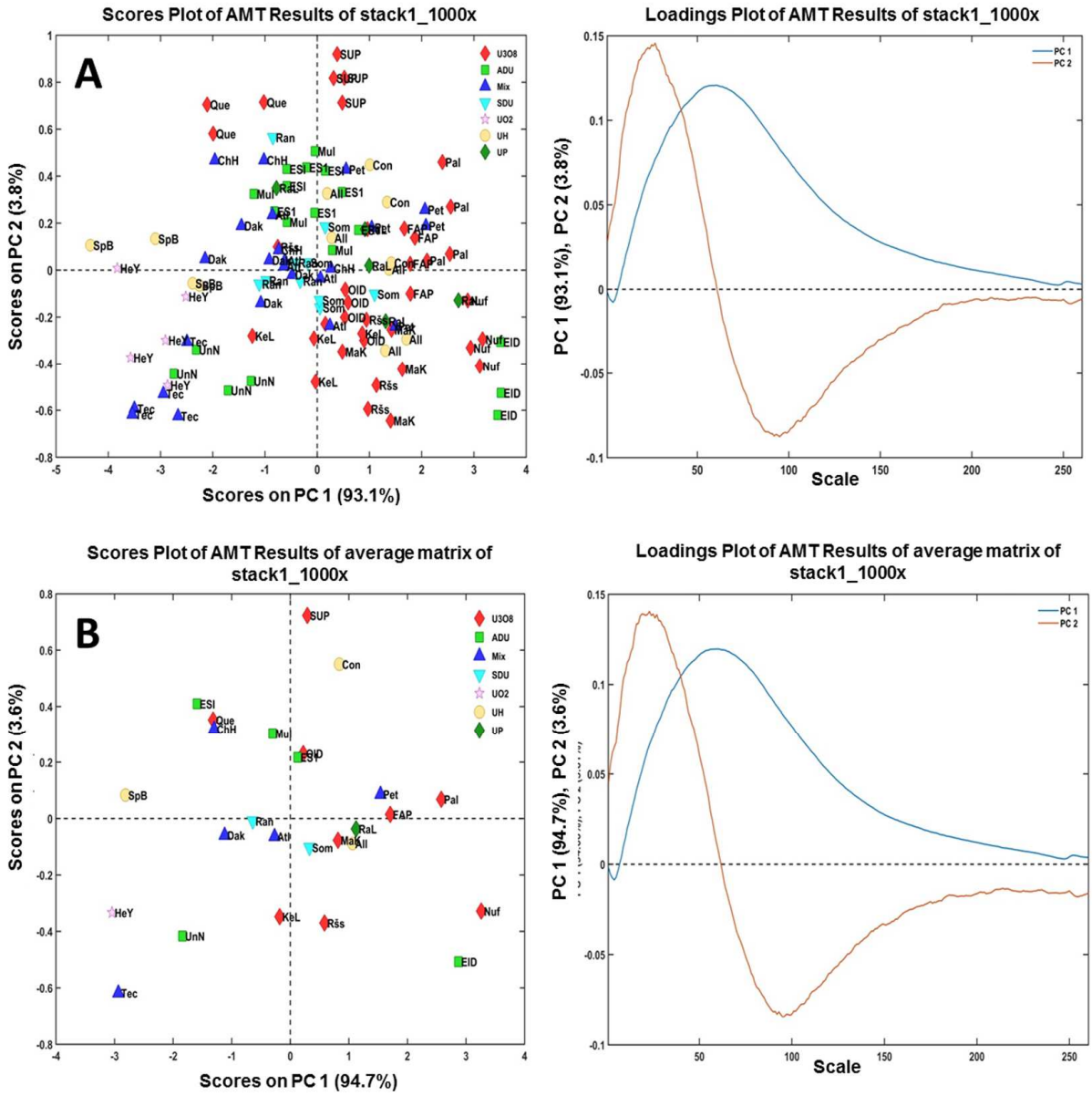

Figure 5. PCA results of the stack1$_{1000x}$: A) scores plot and relative loadings plot of the original matrix; B) scores plot and relative loadings plot of the average matrix.

To better understand the reason for the samples separation, the corresponding MA spectral data shown in Figures 6A, 6B and 6C should be observed directly. The shape of the spectra is typical for isotropic images: at low scales (in this case up to 75) it corresponds to high values of mean angle; thereafter the MA value decreases gradually. Low MA values correspond to low local variation in the image texture complexity (irregularities, roughness, smoothness, graininess, etc.) whereas high MA values indicate significant variations in the image texture complexity [39, 45]. From Figure 6A, showing all the replicates of the MA spectra obtained from the images of stack1$_{1000x}$, it is difficult to identify unequivocal differences among samples or groups of samples associated with the facilities used for the production. The analysis becomes somewhat easier when the average curve of MA spectra for each sample is reported (Figure 6B). Even though the spectra of all the samples have similar patterns, the curves are sufficiently spread apart. To better explain the MA spectra, only six samples and their SEM images are reported in Figure 6C. Two samples (EID and Nuf) are characterised by a smooth surface and the presence of very small grains. Two other samples (MaK and FAP) are characterised by

grains of intermediate size while the other two samples (HeY and Tec) are characterised by rough and irregular surface with big grains. Spectra at low MA values for all the scales correspond to samples with a small variation in the image texture complexity from the local to the global level. On the contrary, the spectra having higher values of mean angle for all the scales correspond to samples having high variation in the image texture complexity, evident by the presence of the small grains and smooth surface of the bulk quantity. When talking about texture it is very important to clearly state if one refers to the **morphology** texture or to the **image** texture because, as in this case, they can exhibit opposite trends.

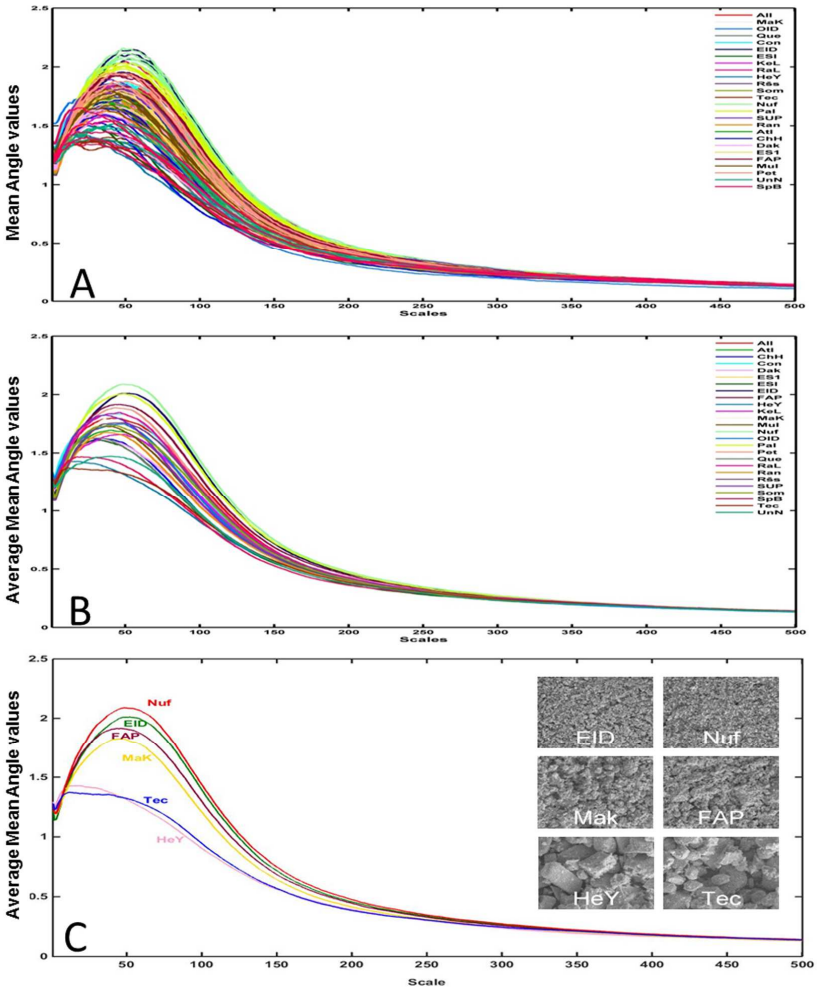

Figure 6. AMT spectral representation. A) spectra of all samples of stack1$_{1000x}$; B) average mean angle spectra of the samples of stack1$_{1000x}$; C) spectra of six selected samples and their relatives images from stack1$_{1000x}$ (EID, Nuf, Mak, FAP, HeY, Tec).

In fact, the images with small grains show a lot of intensity variation in a relative small distance in a specific direction, as can be seen in Figure 7 where the intensity profile of the six images (EID, Nuf, MaK, FAP, HeY and Tec) having different surface aspect (surface appearance) and then different image texture are shown. Looking at the same six samples in the scores plot of Figure 3, the distribution of samples based on their similar 'characteristics' can now be understood.

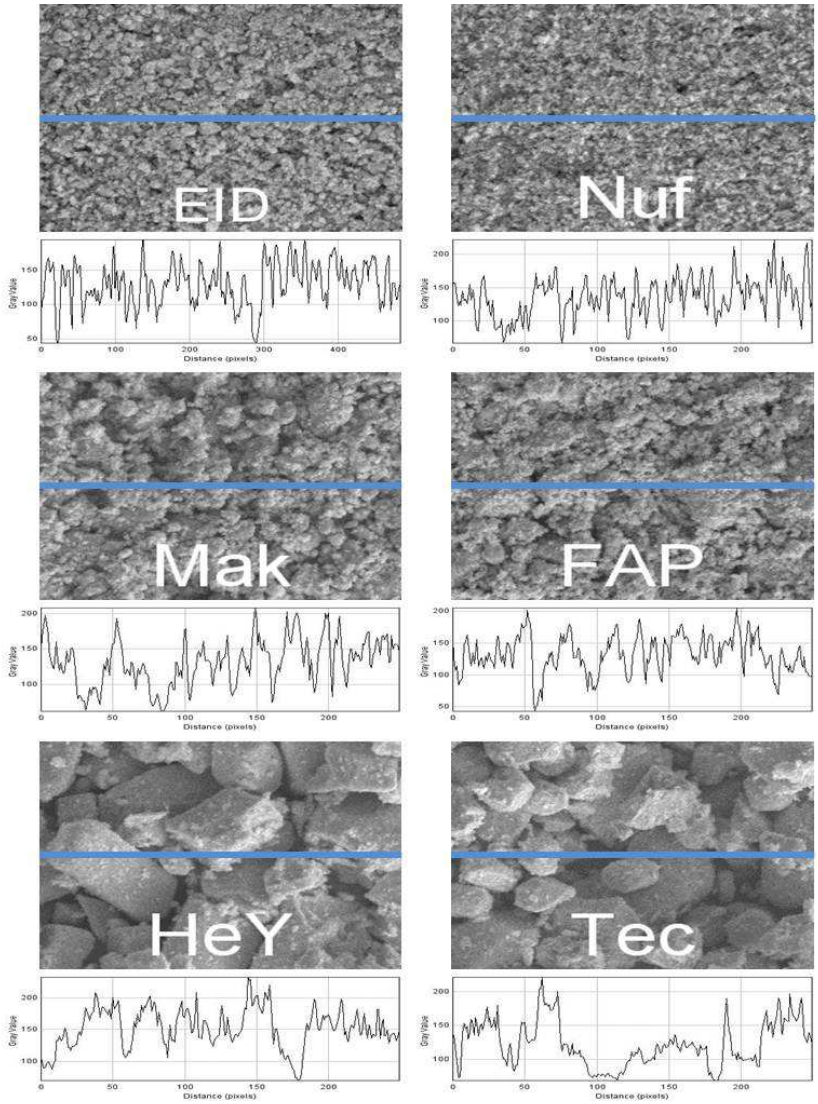

Figure 7. Intensity profile along the blue line of six different samples (EID, Nuf, Mak, FAP, HeY, Tec) having a different surface aspect and then different image texture.

It is noteworthy that, in this work, only the composition and the process technologies used for the production of the different UOCs have been considered as independent factors to distinguish the samples in the scores plots while the loadings plots display the relationship among the variables (in this case the scales). No other information has been taken into account to explain the samples distribution in the scores plots. This explorative analysis has shown how the AMT algorithm is able to distinguish samples produced with the same composition, but by different facilities.

3.2 Results on images at 250× of magnification

The same approach was used on the stacks with the images acquired at 250× magnification. Only the result for stack1 is reported. In this case, it must be considered that the amount of information acquired in the images at 250× magnification is more than that acquired at 1 000× magnification. In other words, the quantity analysed has been more representative of the actual samples. Figure 8A shows the scores plot of PC1-PC2 and the relative loadings plot, while in Figure 8B the scores and the loadings plots obtained from the average matrix are reported. All 26 samples are shown in the scores plot; also in this case, it is possible to identify clusters of the samples TeC, Que, Nuf,

EID, HeY, SpB, Pal, KeL, Pet, Con despite some overlaps. Similar to Figure 5A, samples with a less textured morphology occupy the right part of the scores plot, while the samples characterised by higher textured morphology are on the left part. The first two PCs were enough to explain the samples distribution as a function of their surface characteristics only, with 96.3 % of total explained variance ($PC1_{S1}$=77.0 %; $PC2_{S1}$=19.3 %). The main difference between the results obtained at the two magnifications is that in the image acquired at 1 000× of magnification the image texture is more affected by the morphology of individual particles that can be observed in the images, while at 250× magnification, the texture is more related to the bulk properties of the powder (less details of individual grains can be seen).

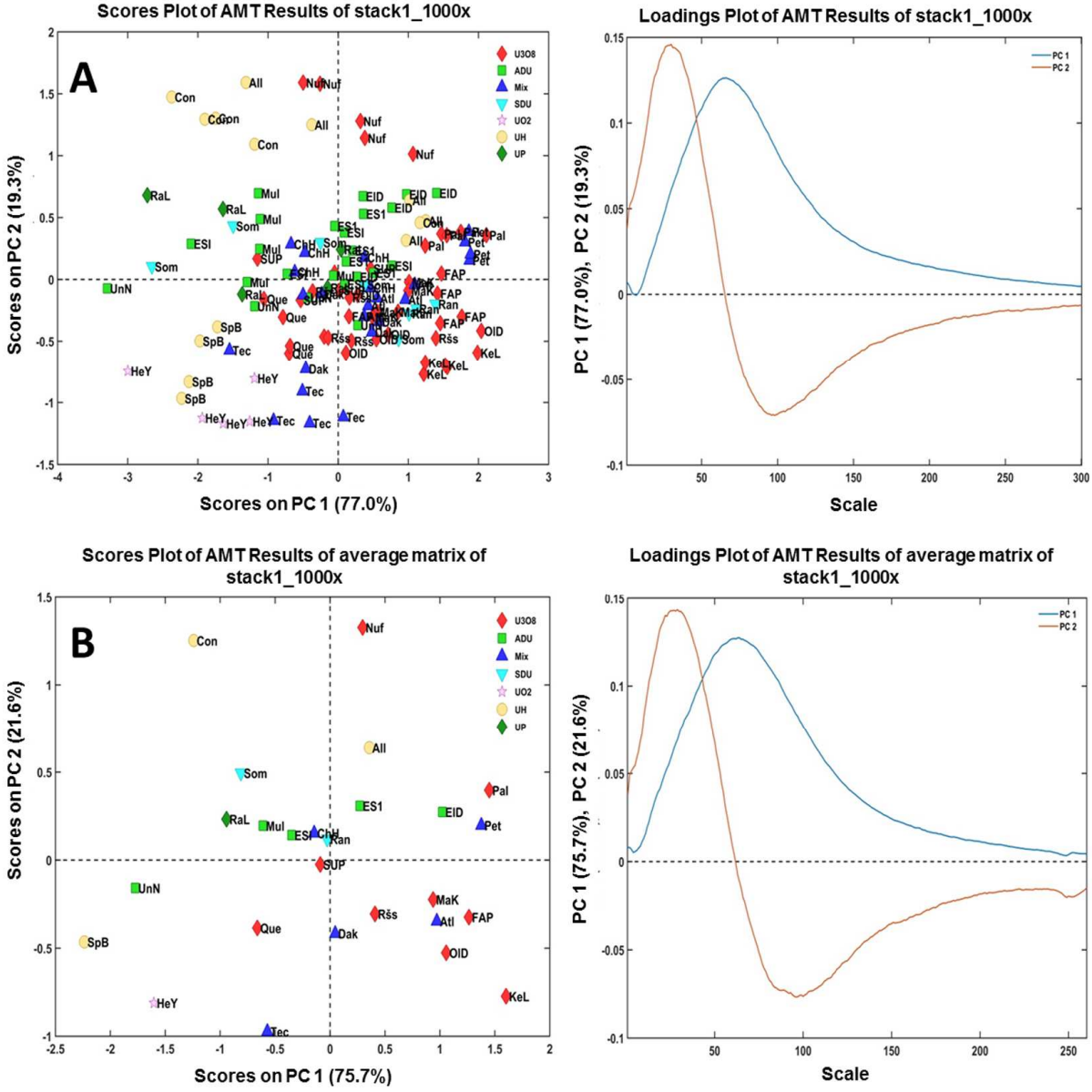

Figure 8. PCA results of the stack1 acquired at 250× of magnification: A) scores plot and relative loadings plot of the original matrix; B) scores plot and relative loadings plot of the average matrix.

4. Conclusion

In this study a new method, the image texture analysis, has been applied to nuclear forensic investigation. In particular the AMT algorithm combined with multivariate data analysis was used to obtain a new fingerprint or new signature, the AMT spectrum, of different UOCs samples from their surface characteristics. The AMT method is based, like other methods (IR/Raman spectroscopy), on the chemo metric approach on multivariate data set obtained directly from the textured images of the samples. The results have shown how PCA provided a view of the distribution of samples in the scores plot and all the samples could be identified. This preliminary research has shown how the AMT algorithm can be used to distinguish samples having the same composition, but produced by different facilities in different countries. The present method could be taken into account as a new tool to obtain rapidly information about nuclear materials under investigation. These quick results could be later compared with the information coming from more time-consuming techniques. The time factor can play an important role in the investigative process to answer questions surrounding interdicted nuclear or radioactive materials. In conclusion, the present image texture analysis method could be considered as an additional valuable instrument in the nuclear research field with a good potential for improvement based on further studies. Future perspectives could include an improvement of the model based on the AMT spectral data for the identification and classification of unknown UOCs samples and the possible use of simpler and faster equipment for image acquisition like the optical microscope or high resolution photo cameras that don’t require sample preparation. This method and this particular application may open a new perspective for nuclear forensics science.

References

[1] Mayer, K., Wallenius, M. and Ray, I., 'Nuclear forensics — a methodology providing clues on the origin of illicitly trafficked nuclear materials', *Analyst* 130 (2005), 433-441.

[2] Wallenius, M., Mayer, K. and Ray, I., 'Nuclear forensic investigations: Two case studies', *Forensic Science International* 156 (2006), 55-62.

[3] Mayer, K., Wallenius, M. and Fanghänel, T., 'Nuclear forensic science — From cradle to maturity', *Journal of Alloys and Compounds* 444-445 (2007), 50-56.

[4] Wallenius, M. et al., 'Nuclear forensic investigations with a focus on plutonium', *Journal of Alloys and Compounds* 444-445 (2007), 57-62.

[5] Varga, Z. et al., 'Analysis of uranium ore concentrates for origin assessment', *Proc. Radiochimica Acta* 1 (2011), 1-4.

[6] Budinger, P. A., Drenski, T. L., Varnes, A. W. and Mooney, J. R., 'The Case of the Great Yellow Cake Caper', *Analytical Chemistry* 52 (1980), 942A-948A.

[7] Keegan, E. et al., 'Nuclear forensic analysis of an unknown uranium ore concentrate sample seized in a criminal investigation in Australia', *Forensic Science International* 240 (2014), 111–121.

[8] Keegan, E. et al., 'The provenance of Australian uranium ore concentrates by elemental and isotopic analysis', *Applied Geochemistry* 23 (2008), 765-777.

[9] Brennecka, G. A., Borg, L. E., Hutcheon, I. D., Sharp, M. A. and Anbar, A. D., 'Natural variations in uranium isotope ratios of uranium ore concentrates: Understanding the 238U/235U fractionation mechanism', *Earth and Planetary Science Letters* 291 (2010), 228-233.

[10] Varga, Z., Wallenius, M., Mayer K. and Hrnecek, E., 'Alternative method for the production date determination of impure uranium ore concentrate samples', *Journal of Radioanalytical and Nuclear Chemistry* 290 (2011), 485-492.

[11] Švedkauskaite-LeGore, J., Mayer, K., Millet, S., Nicholl, A., Rasmussen, G. and Baltrunas, D., 'Investigation of the isotopic composition of lead and of trace elements concentrations in natural uranium materials as a signature in nuclear forensics', *Radiochimica Acta.* 95 (2007), 601-605.

[12] Varga, Z., Wallenius, M., Mayer, K., Keegan, E. and Millet, S., 'Application of Lead and Strontium Isotope Ratio Measurements for the Origin Assessment of Uranium Ore Concentrates', *Analytical Chemistry* 81 (2009), 8327-8334.

[13] Švedkauskaitė-LeGore, J., Rasmussen, G., Abousahl, S. and Belle, P., 'Investigation of the sample characteristics needed for the determination of the origin of uranium-bearing materials', *Journal of Radioanalytical and Nuclear Chemistry* 278 (2008), 201-209.

[14] Han, S.-H., Varga, Z., Krajko, J., Wallenius, M., Song, K. and Mayer, K., 'Measurement of the sulphur isotope ratio (34S/32S) in uranium ore concentrates (yellow cakes) for origin assessment', *Journal of Analytical Atomic Spectrometry* 29 (2013), 1919-1925.

[15] Krajkó, J., Varga, Z., Yalcintas, E., Wallenius, M. and Mayer, K., 'Application of neodymium isotope ratio measurements for the origin assessment of uranium ore concentrates', *Talanta* 129 (2014), 499-504.

[16] Varga, Z., Katona, R., Stefánka, Z., Wallenius, M., Mayer, K. and Nicholl, A., 'Determination of rare-earth elements in uranium-bearing materials by inductively coupled plasma mass spectrometry', *Talanta* 80 (2010), 1744-1749.

[17] Varga, Z., Wallenius, M. and Mayer, K., 'Origin assessment of uranium ore concentrates based on their rare-earth elemental impurity pattern', *Radiochimica Acta International journal for chemical aspects of nuclear science and technology* 98 (2010), 771-778.

[18] Keegan, E., Wallenius, M., Mayer, K., Varga, Z. and Rasmussen, G., 'Attribution of uranium ore concentrates using elemental and anionic data', *Applied Geochemistry* 27 (2012), 1600-1609.

[19] Kennedy, A. K., Bostick, D. A., Hexel, C. R., Smith, R. R. and Giaquinto, J. M., 'Non-volatile organic analysis of uranium ore concentrates', *Journal of Radioanalytical and Nuclear Chemistry* 296 (2013), 817-821.
[20] Badaut, V., Wallenius, M. and Mayer, K., 'Anion analysis in uranium ore concentrates by ion chromatography', *Journal of Radioanalytical and Nuclear Chemistry* 280 (2009), 57-61.
[21] Varga, Z. et al., 'Characterisation and classification of uranium ore concentrates (yellow cakes) using infrared spectrometry', *Radiochimica Acta* 99 (2011), 1-7.
[22] Plaue, J. W., Klunder, G. L., Hutcheon, I. D. and Czerwinski, K. R., 'Near infrared reflectance spectroscopy as a process signature in uranium oxides', *Journal of Radioanalytical and Nuclear Chemistry* 296 (2013), 551-555.
[23] Klunder, G. L., Plaue, J. W., Spackman, P. E., Grant, P. M., Lindvall, R. E. and Hutcheon, I. D., 'Application of Visible/Near-Infrared Reflectance Spectroscopy to Uranium Ore Concentrates for Nuclear Forensic Analysis and Attribution', *Applied Spectroscopy* 67 (2013), 1049-1056.
[24] Sirven, J.-B., Pailloux, A., M'Baye, Y., Coulon, N., Alpettaz, T. and Gosse, S., 'Towards the determination of the geographical origin of yellow cake samples by laser-induced breakdown spectroscopy and chemometrics', *Journal of Analytical Atomic Spectrometry* 24 (2009), 451-459.
[25] Ho, D. M. L. et al., 'Applicability of Raman Spectroscopy as a Tool in Nuclear Forensics for Analysis of Uranium Ore Concentrates', *Radiochimica Acta* 101 (2013), 779-784.
[26] Ho, D. M. L., Jones, A. E., Goulermas, J. Y., Turner, P., Varga, Z., Fongaro, L., Fanghänel, T. and Mayer, K., 'Raman spectroscopy of uranium compounds and the use of multivariate data analysis for visualization and classification', *Forensics Science International 251* (2015), 61-68.
[27] Fongaro, L., Alamprese, C. and Casiraghi, E., 'Ripening of Salami: assessment of colour and aspect evolution using Image Analysis and Multivariate Image Analysis', *Meat Science* 101 (2015), 73-77.
[28] Sabo, E., Beck, A. H., Montgomery, E. A., Bhattacharya, B., Meitner, P., Wang, J. Y. and Resnick, M. B., 'Computerized morphometry as an aid in determining the grade of dysplasia and progression to adenocarcinoma in Barrett's esophagus', *Laboratory Investigation* 86 (2006), 1261-1271.
[29] Van Der Meer, F., Hecker, C., Van Ruitenbeek, F., Van der Werff, H., De Wijkerslooth, C. and Wechsler, C., 'Geologic remote sensing for geothermal exploration: A review', *International Journal of Applied Earth Observation and Geoinformation* 33 (2014), 255–269.
[30] Yang, X. and Knopp, M. V., 'Quantifying tumor vascular heterogeneity with dynamic contrast-enhanced magnetic resonance imaging: a review', *Journal of Biomedicine and Biotechnology* volume 2011(2011), Article number 732848.
[31] Chaudhary, U. K., Iqbal, M. and Ahmad, M., 'Defect sizing of post-irradiated nuclear fuels using grayscale thresholding in their radiographic images', *Nuclear Engineering and Design* 240 (2010), 3455-3461.
[32] Fortunato, D. O. A. et al., 'Automatic defect identification on PWR nuclear power station fuel pellets', *Nuclear Engineering and Design* 245 (2012), 62-77.
[33] Kercher, K. A., Hunn, D. J., Price R. J. and Pappano, P., 'Automated optical microscopy of coated particle fuel', *Journal of Nuclear Materials* 380 (2008), 76-84.
[34] Antoniou, I., Ivanov, V. V., Kostenko, B. F., Spino, J. and Stalios, A. D., 'Fractal analysis of high burn-up structures in UO2', *Chaos, Solitons and Fractals* 19 (2004), 731-737.
[35] Woong, K. K., Young, W. L., Moon, S. C., Park, J. Y., Woong, S. R. and Park, J. B., 'Nondestructive measurement of the coating thickness for simulated TRISO-coated fuel particles by using phase contrast X-ray radiography', *Nuclear Engineering and Design* 238 (2008) 3285-3291.

[36] Yang, M., Zhang, J., Song, S.-J., Li, X., Meng, F., Kang, T., Liu, W. and Wei, D., 'Imaging and measuring methods for coating layer thickness of TRISO-coated fuel particles with high accuracy', *NDT&E International* 55 (2013), 82–89.
[37] Ho, D. M. L., Manara, D., Varga, Z., Fongaro, L., Nicholl, A., Berlizov, A., Lindqvist-Reis, P., Fanghänel, T. and Mayer, K., 'Exploring spectroscopic and morphological data as new signatures for uranium ore concentrates', Conference Paper, IAEA Nuclear Forensics Conference, Vienna, Austria, 2014.
[38] Hidalgo, A., Fongaro, L. and Brandolini, A., 'Wheat flour granulometry determines colour perception', *Food Research International* 64 (2014), 363-370.
[39] Huang, J. and Esbensen, K. H., 'Applications of Angle Measure Technique (AMT) in IA Part I. A new methodology for in situ powder characterization', *Chemometrics and Intelligent Laboratory Systems* 54 (2000), 1-19.
[40] Andrle, R., 'The Angle Measure Technique: A New Method for Characterizing the Complexity of Geomorphic Lines', *Geophysics* 26 (1994), 83-97.
[41] Esbensen, K. H., Hjelmen, K. H. and Kvaal, K., 'The AMT approach in chemometrics — first forays', *Journal of Chemometrics* 10 (1996), 569-590.
[42] Rasband, W. S., ImageJ, U. S. National Institutes of Health, Bethesda, Maryland, USA, http://imagej.nih.gov/ij, 1997-2012, (Accessed on 18 September 2014).
[43] Kucheryavski, S. V., Kvaal, K., Halstensen, M., Mortensen, P. P., Dahl, C. K., Minkkinen, P. and Esbensen, K. H., 'Optimal corrections for digitization and quantification effects in angle measure technique (AMT) texture analysis', *Journal of Chemometrics* 22 (2008), 722-737.
[44] Bharati, M. H., Liu, J. J. and MacGregor, J. F., 'Image texture analysis: methods and comparisons', *Chemometrics and Intelligent Laboratory Systems* 72 (2004), 57-71.
[45] Fongaro, L. and Kvaal, K., 'Surface texture characterization of an Italian pasta by means of univariate and multivariate feature extraction from their texture images', *Food Research International* 51 (2013), 693-705.
[46] Haralick, R. M., Shanmugam, K. and Dinstein, I., 'Textural features for image classification', IEEE Transactions on Systems, *Man and Cybernetics* 3 (1973), 610-321.
[47] Huang, J. and Esbensen, K. H., 'Applications of AMT (Angle Measure Technique) in IA Part II: Prediction of powder functional properties and mixing components using Multivariate AMT Regression (MAR)', *Chemometrics and Intelligent Laboratory Systems* 57 (2001), 37-56.
[48] Kucheryavski, S. and Belyaev, I., 'Classification and analysis of non-isotropic images by Angle Measure Technique (AMT) with contour unfolding', *Analytica chimica acta* 642 (2009), 135-141.
[49] Kvaal, K., Wold, J. P., Indahl, U. G., Baardseth, P. and Næs, T., 'Multivariate feature extraction from textural images of bread', *Chemometrics and Intelligent Laboratory Systems* 42 (1998), 141-158.
[50] Mortensen, P. P. and Esbensen, K. H., 'Optimization of the Angle Measure Technique for image analytical sampling of particulate matter', *Chemometrics and Intelligent Laboratory Systems* 75 (2005), 219-229.
[51] Kvaal K., Kucheryavski, S. V., Halstensen, M., Kvaal, S., Flø, A. S., Minkkinen, P. and Esbensen, K. H., 'eAMTexplorer: a software package for texture and signal characterization using Angle Measure Technique', *Journal of Chemometrics* 22 (2008), 717-721.
[52] Kvaal, K., *jAMTexplorer user guide*, 2014.
[53] Martens, H. and Naes, T., *Multivariate calibration*, Wiley & Sons, 1989.
[54] Indahl U. G., Martens, H. and Naes, T., 'From dummy regression to prior probabilities in PLS-DA', *Journal of Chemometrics* 21 (2007), 529-536.
[55] Wise, B. M., Bro, R., Shaver, J. M., Windig W. and Koch, R. S., PLS_Toolbox Version 4.0 for use with MATLAB, Eigenvector Research, Inc. WA, USA, 2006.
[56] De La Ossa M. A. F., Garcia-Ruiz, C. and Amigo, J. M., 'Near infrared spectral imaging for the analysis of dynamite residues on human handprints', *Talanta* 130 (2014) 315-321.

List of abbreviations and definitions

AMT, Angle measure technique; C, Calibration; CV, Cross-validation; I, Intensity; IA, Image analysis; PCA, Principal component analysis; PLS-DA, Partial least square discriminant analysis; RMSE, Root mean square error; UOCs, Uranium ore concentrates.

List of figures

List of tables

Europe Direct is a service to help you find answers to your questions about the European Union
Free phone number (*): 00 800 6 7 8 9 10 11
(*) Certain mobile telephone operators do not allow access to 00 800 numbers or these calls may be billed.

A great deal of additional information on the European Union is available on the internet.
It can be accessed through the Europa server http://europa.eu

LC-NA-27979-EN-N

JRC Mission

As the Commission's in-house science service, the Joint Research Centre's mission is to provide EU policies with independent, evidence-based scientific and technical support throughout the whole policy cycle.

Working in close cooperation with policy directorates-general, the JRC addresses key societal challenges while stimulating innovation through developing new methods, tools and standards, and sharing its know-how with the Member States, the scientific community and international partners.

Serving society
Stimulating innovation
Supporting legislation

Publications Office

doi: 10.2789/851269

ISBN 978-92-79-59538-7